

Hertzian contact fatigue on alumina/alumina-zirconia laminated composites

E. Jiménez-Piqué^{a,*}, L. Ceseracciu^a, F. Chalvet^b, M. Anglada^a, G. de Portu^b

^a *Departamento de Ciencia de Materiales e Ingeniería Metalúrgica, Universitat Politècnica de Catalunya, Avda. Diagonal 647 (ETSEIB), 08028 Barcelona, Spain*

^b *National Research Council (CNR), Institute of Science and Technology for Ceramics (ISTEC), 48018 Faenza (RA), Italy*

Received 11 July 2004; accepted 27 August 2004

Abstract

The Hertzian contact fatigue of two $\text{Al}_2\text{O}_3/\text{Al}_2\text{O}_3\text{-ZrO}_2$ laminated composites with different layer thickness and, consequently, different residual stress at the surface, was studied both under cyclic loading and under static loading (stress corrosion cracking). The apparition of a superficial ring crack, considered as the first stage of damage, was recorded as a function of time or number of cycles. A monolithic alumina processed in a similar way than the composites and with comparable microstructure was also tested for comparison purposes. Results show that the laminated composites present better resistance to contact fatigue than monolithic alumina. Comparison between static and cyclic loading data reveals that the alumina suffers from fatigue, and not only from stress corrosion cracking under cyclic loading. This fatigue is attributed to grain bridging degradation of alumina. A simple relationship between indentation load and time for apparition of ring crack, based on the Paris law, is derived, yielding values of the exponents similar to values previously reported in the literature.

© 2004 Elsevier Ltd. All rights reserved.

Keywords: Fatigue; Toughness; Laminated composites; Al_2O_3 ; ZrO_2

1. Introduction

Ceramic composites based in layered architectures have proven to be excellent structural ceramics due to their increase in fracture energy, apparent fracture toughness, faculty to arrest cracks and, consequently, reliability.^{1–3} This increase in mechanical properties can be achieved through different strategies such as weak interfaces,⁴ containment of martensitic transformation,⁵ existence of porous layers⁶ or introduction of compressive stresses.^{7,8} This latter approach is one of the most usual ones, and it is normally achieved by stacking alternating layers of materials with different thermal expansion coefficients that will translate in residual stresses during cooling in the sintering stage. In some cases, residual stresses can also be introduced by other means such as phase transformation.⁹ In this case, the interface between the layers

is normally well bonded, and the increase in fracture toughness and fracture energy is achieved through the existence of residual stresses and the crack deflection caused by the elastic mismatch between the different materials.¹⁰ Among the ceramic laminated composites that can be produced, one of the most preferred material combinations is alumina and zirconia. Usually, at least one of the layers of the composite is made of an alumina-zirconia composite, in order to tailor the coefficient of thermal expansion (CTE) and, consequently, the residual stresses. In this way, the channel cracking produced during sintering can be avoided. The reason for choosing alumina and zirconia as the constituent materials of ceramic laminates is generally because of the excellent bonding between the layers in the absence of excessive diffusion between components, their good thermo-mechanical properties and their relatively ease of processing.

There have been several studies about fracture behaviour of these materials, specially about fracture toughness measurement and crack propagation through the layers.^{11,12} All

* Corresponding author. Tel.: +34 934054454; fax: +34 934016706.

E-mail address: emilio.jimenez@upc.es (E. Jiménez-Piqué).

these studies have shown that these multilayer ceramic composites present better fracture properties than their monolithic counterparts and that, in some cases, they mitigate the brittleness of the ceramics by presenting a “graceful failure” behaviour. Among these improvements of toughness, one of the most interesting results is the one obtained by Rao et al.,¹³ where they demonstrated that certain laminates that present a, usually thin, layer under high residual stress, can show a threshold strength: that is, the strength of the material becomes insensitive to the length of the initial crack. The value of this threshold strength can be increased by inducing crack bifurcation when the crack enters the compressive layer.¹⁴

Despite of the considerable effort done in characterizing the mechanical properties of these laminated composites, most of the studies deal with crack propagation through layers, usually in bending tests, there is still not much research done about the behaviour of these materials under repetitive and/or sliding surface loads, which in some cases may be closer to real-life applications. This is particularly true in cases such as biomedical implants or bearings, where ceramics are used because of their biocompatibility and good tribological behaviour. In previous studies,¹⁵ some of the authors have already shown that ceramic laminates of Al_2O_3 and $\text{Al}_2\text{O}_3\text{-ZrO}_2$ do present improved wear resistance and reduced friction coefficient when compared to pure alumina, due to the residual stresses introduced during processing. The aim of this work is then to investigate the contact fatigue response of symmetrical laminated ceramics of Al_2O_3 and $\text{Al}_2\text{O}_3\text{-ZrO}_2$ with compressive residual stresses at the surface. For that purpose, cyclic and static Hertzian indentation tests have been carried out, and the response of the laminates have been compared to the response of a stress-free alumina.

Hertzian indentation presents the advantage over sharp indentations in the fact that damage in the material can be produced in most of the cases without appreciable plastic deformation, which simplifies the analysis because fracture can occur within an elastic field. Moreover, Hertzian indentations resemble more closely the real contact that the material is expected to suffer in service. In recent years, there have been several studies on Hertzian contact fatigue on ceramics, where the degradation of the material under cyclic loading have been evaluated by measuring the damaged strength of the material.^{16–18} The damage produced in the ceramic materials was either cone cracking or quasi-plasticity, depending on the material type and the size of the microstructure. In this work, we present the Hertzian fatigue of a ceramic laminate, and the degradation of the material is measured by observing the apparition of superficial ring crack, without any strength measurements.¹⁹ The reason for that is twofold: first, in this way, a larger amount of measurements can be done with a relatively small amount of material; and, second, the behaviour of the different laminated composites can be compared directly, which could be more cumbersome if the strength was evaluated, because of the different behaviour under non-local load of the laminated materials.

2. Experimental

2.1. Material processing

To obtain the ceramic sheets suitable for the preparation of laminated composites, two powders were used:

- high purity (99.7%) alumina (Alcoa A16-SG, Alcoa Aluminum Co., New York, USA) with an average particle size of $0.3\ \mu\text{m}$,
- tetragonal zirconia polycrystals (TZ3Y-S, Tosho Corp., Japan) containing 94.7% of ZrO_2 and 3 mol% of Y_2O_3 (usually referred to as 3Y-TZP) with an average particle size of $0.3\ \mu\text{m}$.

The different powders were mixed with organic binders, dispersant, plasticizers and solvents to obtain suitable slips for tape casting. After mixing with organic components, the slurry containing the ceramic powders was tape casted onto a mylar sheet moved at a constant speed of 200 mm/min. Detail on this technique can be found elsewhere.²⁰

Sheets of pure alumina (hereinafter designated “A”) as well as of the composite alumina-zirconia (hereinafter designated “AZ”) in the volume ratio 60/40 were prepared. The thicknesses of the green tapes were selected in order to obtain, after sintering, layers of about $200\ \mu\text{m}$ (A) and $250\ \mu\text{m}$ (AZ). After drying, laminae of $50\ \text{mm} \times 34\ \text{mm}$ were cut from the different ceramic sheets. Hybrid laminates were prepared by stacking and warm pressing the green sheets at $75\ ^\circ\text{C}$ at a pressure of 30 MPa for 30 min. Different samples were obtained by alternately superimposing one layer of alumina and one layer of alumina-zirconia (this structure is hereinafter designated A/AZ) or one layer of alumina and two layer of alumina-zirconia (hereinafter designated A/2AZ). The structures were designed in order to have always an alumina layer in both the outer surfaces. Debonding was carried out with a very slow heating rate up to $600\ ^\circ\text{C}$, followed by sintering at $1550\ ^\circ\text{C}$ for 1 h. We thus obtained dense samples (97% of theoretical density) with a thickness of about 3.0 mm, containing layers with a thickness ratio of about 1/1.3 (A/AZ) and 1/2.6 (A/2AZ). In the hybrid samples, due to lower thermal expansion coefficient and shrinkage during sintering, the external alumina layers undergo residual compressive stresses. As reference material (i.e. nominally stress free), pure monolithic alumina (MA) was prepared by cold isostatic pressing and sintering at $1550\ ^\circ\text{C}$ for 1 h.

2.2. Mechanical tests

Once the laminated plates were produced, they were cut into prismatic bars of about $4\ \text{mm} \times 3\ \text{mm} \times 20\ \text{mm}$ with a diamond saw. The top layer of alumina (which was in compression) was polished with diamond suspension up to $3\ \mu\text{m}$ with a low applied force in order to avoid excessive loss of material ($30\ \mu\text{m}$ at most), and to produce a similar surface flaw size distribution for all the samples. Several samples were polished in the cross section area and thermally etched

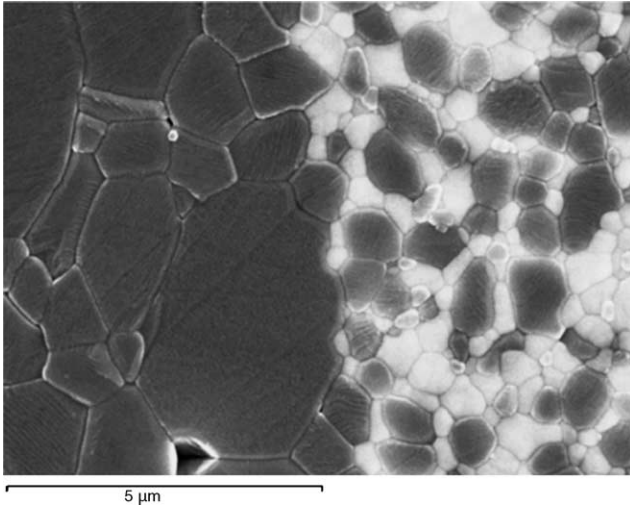


Fig. 1. SEM pictures of the interface between alumina and alumina-zirconia layers of an A/AZ laminated composites. It can be observed that the interface is well bonded, and that the alumina grains in the alumina-zirconia composite have a smaller grain size, due to the constraint of the zirconia grains.

(1500 °C, 30 min) for observing the microstructure of the material nearby the interface. Fig. 1 shows the SEM picture of the interface between two layers of alumina and alumina-zirconia, where it can be observed that the interface is well bonded. MA samples were prepared in the same way, and their microstructure was also observed by SEM. The grain size of the alumina layers of the laminates and the monolithic alumina was measured to be $1.9 \pm 0.7 \mu\text{m}$ for the alumina layers of the ceramic laminates and $1.1 \pm 0.8 \mu\text{m}$ for the MA using the average feret method. The fact that the grain sizes are similar, together with the fact that both the laminates and the MA materials were produced in a similar way, suggest that the materials are similar at the microstructural level, and that any difference in the mechanical behaviour can be attributed to the differences in residual stresses produced by the laminated architecture.

Vickers hardness measurements were carried with different loads (200 g, 300 g, 500 g, 1 kg). For this load range, hardness proved independent of load, and therefore no size-effect was found, as expected. In the A/AZ laminate, measurements of hardness were performed at the top surface, perpendicular to the interface. To measure the hardness in the AZ layer, the top A layer was carefully removed by grinding and polishing on both sides of the sample in order to avoid unbalanced stresses. The mean hardness values of the alumina-zirconia was $H_V^{AZ} = 15.1 \pm 0.7 \text{ GPa}$ and the hardness of the alumina was found to be $H_V^A = 16.9 \pm 0.5 \text{ GPa}$. In the monolithic alumina the hardness was $H_V^A = 16.7 \pm 0.9 \text{ GPa}$. It can be seen that both the MA and the alumina layer presents comparable values of hardness.

Fracture toughness of both MA and A/AZ (measured in the top alumina layer, so the interface was located below the indentation, and perpendicular to the indentation load) was evaluated by measuring the crack lengths produced by a Vickers

indentation of 10 kg and assuming that the crack produced was penny-shape. The fracture toughness of the AZ layers was not measured because their thickness was too small for producing suitable crack lengths without reaching the interface. Also, the fracture toughness of the A/2AZ composite was not measured because Vickers indentations produced excessive chipping in the material due to the higher compressive residual stress.

Acknowledging that the values obtained in this way have to be considered as approximate due to the limitations of the method, the fracture toughness (K_{Ic}) was then evaluated through:²¹

$$K_{Ic} = \chi \frac{P}{c^{3/2}} \quad (1)$$

where P is the load, c the crack length and χ equals 0.08 for this material. Substituting the values of the measured crack lengths, the fracture toughness obtained for both materials were:

$$\begin{aligned} K_{Ic}^A &= 3.5 \pm 0.8 \text{ MPa m}^{1/2} \\ K_{Ic}^{A/AZ} &= 6.0 \pm 0.8 \text{ MPa m}^{1/2} \end{aligned} \quad (2)$$

The value of the A/AZ has to be taken as an apparent value, as there the intrinsic toughness is influenced by the residual stresses. Those can be calculated by evaluating the contributions of the intrinsic toughness (K_{Ic}^0 , equal to K_{Ic}^A) and the residual stresses (σ_{res}) as:

$$K_{Ic} = \chi \left(\frac{P}{c_0^{3/2}} \right) + Y \sigma_{res} \sqrt{c_1} \quad (3)$$

from where:

$$Y \sigma_{res} \sqrt{c_1} = K_{Ic}^{A/AZ} - K_{Ic}^A \quad (4)$$

where c_1 is the crack length in the stressed material (A/AZ), c_0 is the crack length in the non-stressed material (MA) and $Y=1.29$ is the geometrical factor. The residual stress was then found to be 183 MPa. By geometrical considerations, the residual stress at the A/2AZ material can be estimated to be 220 MPa. Again, it has to be pointed out that these results are only approximated, because of the limitations of the above-described methods, and that better measurements of the residual stresses can be obtained by other techniques, specially spectroscopic techniques (micro-Raman, XRD, etc.). Despite the limitations, the results obtained here are very similar to previous results described elsewhere.¹⁵

Hertzian contact loads were applied on the laminated composites and in the reference MA material. This was carried out at the top layer with a WC-Co spherical indenter of 2.5 mm. As expected, due to the relative small grain size of the alumina, the main mechanism for damage showed to be cone cracking, and, for that particular indenter size, the critical load for cone cracking was $P_c^A = 607 \pm 50 \text{ N}$ for the alumina and $P_c^{A/AZ} = 675 \pm 50 \text{ N}$ for the A/AZ (top alumina layer).

In evaluating the fatigue behaviour of ceramics, that is, their degradation under repetitive loads below a critical load, it is important to evaluate also their resistance to static loads of the same magnitude that the applied cyclic load. This is due to the fact that ceramic materials are especially prone to stress corrosion cracking enhanced by water vapour, which acts in the existing crack tips when the maximum stress intensity factor is applied and the crack is completely open. In fact, in some cases, the apparent degradation of a ceramic material under cyclic loading can be solely attributed to stress corrosion cracking, discarding, thus, any influence in the degradation of the cyclic loading,²² although this is not the case for alumina. It is important, therefore, to differentiate both mechanisms and compare the degradation under cyclic and static loading.

Hence, in order to evaluate the existence of stress corrosion cracking, indentation tests under constant load for different holding times were performed. In these tests, the material, either alumina, A/AZ or A/2AZ was indented with a WC-Co sphere of 2.5 mm of diameter with an applied load lower than the critical load. The apparition or not of damage was annotated for a set of different times, delimitating a range of times where the initiation of damage was highly probable for that given load. It was considered that damage appeared after observation of a well-developed ring crack^{23–25} in the surface of the sample. The tests were performed in an electromechanical universal test machine (Instron 8562) with a 5 kN load cell. In Fig. 2, the results for A/AZ, A/2AZ laminated composites and MA are presented. In this plot, the open points mean that no appreciable damage was found at that time, while the filled symbol means that a fully developed ring crack was found at that given time and load. Because of the statistical distribution of initial defects in ceramics, which translates in a scatter in strength, the ranges reported do not have to be considered as exact ranges, but only approximated and eval-

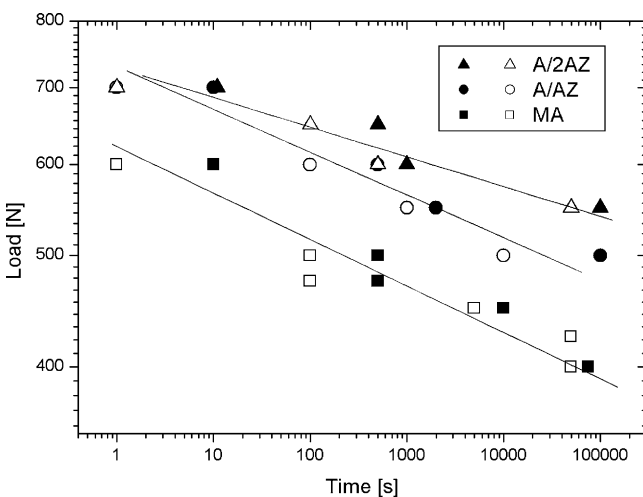


Fig. 2. Applied indenter load against time for a stress corrosion cracking tests for the three materials. Empty points indicate no apparent damage on the surface of the sample, while closed points indicate the existence of a well-developed ring crack.

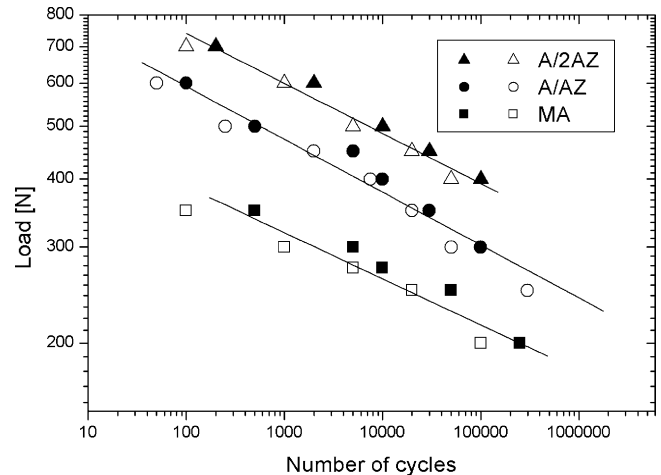


Fig. 3. Applied indentation load against number of cycles of the cyclic loading fatigue tests for MA, A/AZ and A/2AZ materials. Empty points indicate no apparent damage on the surface of the sample, while closed points indicate the existence of a well-developed ring crack.

uated by a limited amount of samples (typically 10). In some cases, some partial ring cracks were observed when times in between ranges were evaluated, which can be attributed to the fact that the crack has grown enough to become visible, but not to a full extent yet.

Cyclic contact tests were performed in a similar way than the static contact tests: samples were indented with a WC-Co sphere of 2.5 mm in diameter in a universal servohydraulic test machine (Instron 8500). Care was taken to properly hold the specimen in order to avoid small displacements and, consequently, fretting fatigue. The WC-Co sphere was periodically inspected for damage, and rotated or replaced when some damage or deformation was observed in the sphere. The applied load was sinusoidal with a frequency of 10 Hz, a constant minimum load of 50 N, and a given maximum load ($R = \sigma_{\min}/\sigma_{\max} = 0.25-0.07$).

In Fig. 3, the occurrence of ring crack is presented as a function of applied maximum load and number of cycles, for both the alumina and the ceramic laminates. The same procedure for damage evaluation under static loading was applied: a series of tests at the same load but with different number of cycles were performed and the surface was examined for the appearance of a well-developed ring crack.

Additional cyclic tests with the same frequency and indenter size and material were performed in the A/AZ material with constant amplitude of loading, $\Delta P = 200$ N, and varying the maximum load from 400 to 600 N ($R = 0.125-0.083$), following the same procedure for damage evaluation as described above, together with tests with a fixed maximum load of $P = 500$ N, and varying amplitude loading from 50 to 300 N. The results of both tests are presented in Fig. 4, where plot in Fig. 4a is the constant amplitude test and plot in Fig. 4b is the constant maximum load test.

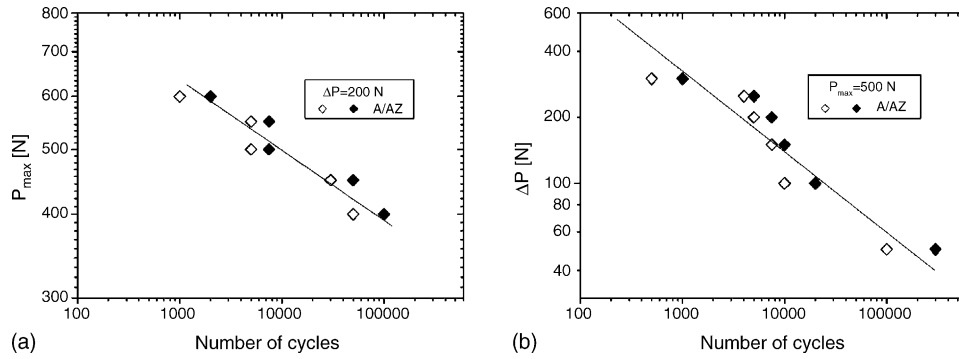


Fig. 4. Cyclic loading tests of A/AZ laminate composite with: (a) difference between maximum and minimum load constant, with maximum applied load against number of cycles; (b) constant maximum load, with ΔP against applied number of cycles.

3. Discussion

After assessment of the results presented in Figs. 2 and 3, it can be seen that the laminated composites present a better resistance to damage than pure alumina, both under constant and cyclic loading. Moreover, it can be seen that, in both cases, A/2AZ presents better results than A/AZ. This can be correlated to the existence of compressive residual stresses at the surface in the laminated materials, being the A/2AZ material the one with the highest magnitude of residual stresses. Additionally, it is seen that the relationship between load and time or number of cycles may be adjusted by a power–law relationship. The slope of the log–log representation of the data remains comparable for all three materials, and the data is only displaced upwards with increasing residual stress at the surface of the material. There is however a slight disagreement with the A/2AZ material, which can be attributed to the experimental scatter produced at high loads and low times. The fact that the slopes are comparable, suggests that the micromechanisms of damage in all the materials are equivalent, and that the compressive residual stress decreases the apparent stress intensity factor. This equivalent behaviour is consequent with the fact that all materials have a comparable microstructure and therefore, the chemical and microstructural mechanisms that provoke damage can be considered as similar for the laminates and the MA.

In the case of static loading the mechanisms of degradation can be attributed to stress corrosion cracking: when the load is applied, the natural flaws are opened and water vapour penetrates to the crack tip, where it reacts with the glass particles of the alumina thus diminishing the strength of the material and enlarging the crack.²⁶

It is also seen that all three materials under cyclic loading present damage much earlier than under static loading. This is better seen in Fig. 5, where the behaviour under both static and cyclic loading of the A/AZ composite is presented, and where the number of cycles of cyclic loading have been converted into equivalent time (t_{eff}), defined as:

$$t_{\text{eff}} = G_c \frac{N}{f} \tag{5}$$

where N is the number of cycles, f is the frequency of the test (10Hz in our case) and G_c is a translation constant that takes into account the effective time when the stress intensity factor is above the threshold value for stress corrosion cracking. In Fig. 5, the value of G_c has been taken equal to 0.1,²⁷ corresponding to a subcritical crack growth exponent of 30.

If the same degradation mechanism was operating under cyclic and static loading, the experimental results of both cyclic and static loading will be equal after conversion of number of cycles into effective time. In this case, no fatigue effect will appear during cyclic loading. However, this is not the case, as cyclic loading produces damage much earlier than static loading. Moreover, it has to be noted that degradation under cyclic loading is higher than under static loading even if the effective time was defined as the total time of the test, N/f ($G_c = 1$), assuming the limit case where stress corrosion cracking is acting all the time despite that the crack opening is always smaller.

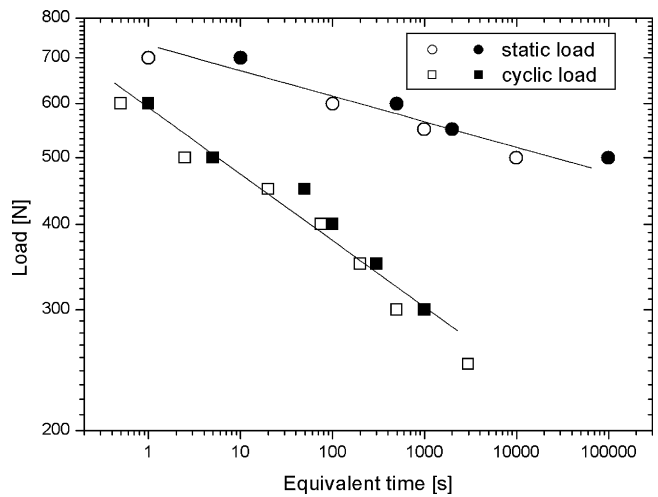


Fig. 5. Comparison between the damage evolution of the static loading and the cyclic loading, represented as applied load against equivalent time, for the A/AZ laminated composite. It is seen how the material suffers a much faster damage under cyclic loading than under static loading. The same behaviour is observed with the other materials.

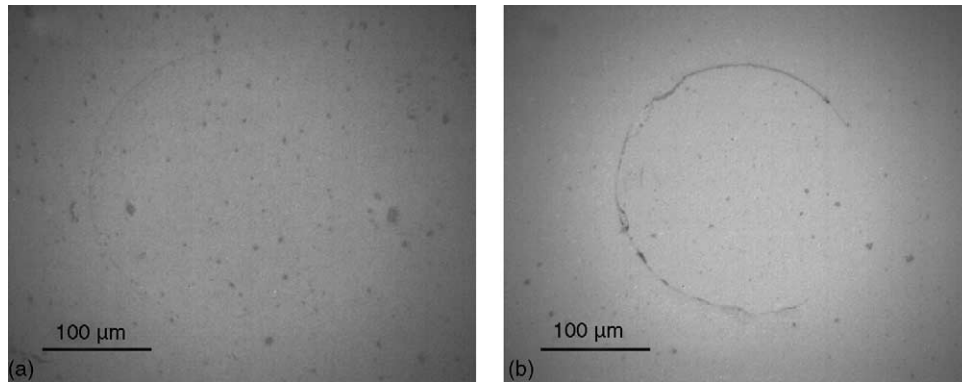


Fig. 6. Optical pictures of typical ring cracks of A/AZ material produced under: (a) static loading and (b) cyclic loading. Ring crack in panel (b) is not perfectly circular and regions of grain bridging are seen.

It then appears to be a real fatigue effect consequence of the cyclic loading and the degradation observed is not just due to the stress corrosion cracking, in accordance with previous studies in alumina.^{28–31} Moreover, the crack growth rate in our systems may be larger than the growth rate measured in larger specimen configurations because the fatigue effect can be enhanced by a short crack effect. This short crack effect is due to the fact that the crack is shorter than the fracture process zone, defined as the volume where the crack-tip shielding mechanisms occur, that are the responsible for the R-curve behaviour. In the case of alumina, the main toughening mechanism is grain bridging.^{32,33} In the case of Hertzian indentation, the crack is short not only in the perimeter direction of the ring, but specially in the depth direction, as the crack is just some micrometers deep because of the sharp decrease in tensile radial stress with depth, which becomes compressive just after a short depth.^{23,34,35} That is, while in the case of stress corrosion cracking the fracture process zone develops without impediment, in the case of cyclic loading this fracture process zone degrades continuously, preventing the development of R-curve. The fatigue effect can be clearly seen in Figs. 6 and 7, where the Hertzian crack produced under subcritical static loading (Fig. 6a and Fig. 7a) and cyclical loading (Fig. 6b and Fig. 7b) are presented, observed by optical and SEM microscopy, respectively. In Fig. 6a and Fig. 7a,

it is appreciated that the crack runs smoothly, while in Fig. 6b and Fig. 7b it is appreciated that the crack runs tortuously, which indicates that the bridging in that region of the crack have degraded through grain sliding²⁸ and rotation.³¹

In Hertzian indentation, it is assumed that the ring crack grows at a distance from the contact radius starting from a flaw at the surface of the material. This ring crack is assumed to be semi-elliptical, of length $2c$ and depth a . After the analysis of Warren and coworkers,^{36,37} the stress intensity factor (K_I) at the surface in the c -direction for a material without residual stress can be expressed as:

$$K_I = p_0 \sqrt{\pi r_0} \left(\mu \sqrt{\frac{a}{r_0}} \right) \quad (6)$$

where p_0 is the peak pressure under the sphere given by:

$$p_0 = \frac{3P}{2\pi r_0^2} \quad (7)$$

with P the applied load, and r_0 the contact radius. This radius can be expressed as function of the load, the radius of the indenter sphere R and the composite Young modulus indenter-material E^* , as:

$$r_0 = \left(\frac{3RP}{4E^*} \right)^{1/3} \quad (8)$$

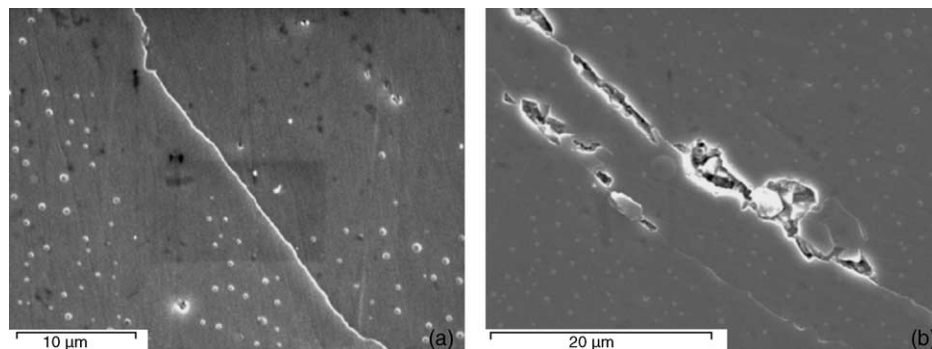


Fig. 7. SEM pictures of typical ring cracks of A/AZ material produced under: (a) static loading and (b) cyclic loading. Observe that the crack in panel (a) is smooth, while in panel (b) the grain removal typical from fatigue mechanisms of ceramics is evident.

with:

$$\frac{1}{E^*} = \frac{1 - \nu_m^2}{E_m} + \frac{1 - \nu_i^2}{E_i} \quad (9)$$

being E and ν the Young's modulus and Poisson ratio of the material (subscript m) and the indenter (subscript i). The function μ is a dimensionless function that depends on the relative crack position, Poisson ratio of the material, crack ellipticity and crack depth. Combining Eqs. (6)–(8), the stress intensity as a function of the applied indentation load can be expressed as:

$$K_I = \left(\frac{3E^*P}{\pi R} \left(\mu \sqrt{\frac{a}{r_0}} \right)^2 \right)^{1/2} \quad (10)$$

The function μ changes as the crack grows. It has to be noted that during the crack growth, the stress intensity factor in the c -direction is larger than the stress intensity factor in the a -direction, and only in some cases $K_{Ia} = K_{Ic}$, when the crack grows in both directions. However, as the crack progresses in the depth direction, the value of μ changes drastically and the c -direction is favoured again. That implies that ring cracks penetrate only slightly on the material while they grow through the perimeter.

The subcritical crack growth rate (dc/dt) can be related to the applied stress intensity factor through a logarithmic relationship:

$$\frac{dc}{dt} = v_0 \left(\frac{K_I}{K_{Ic}} \right)^n \quad (11)$$

where v_0 is a material-dependant constant, n is the crack velocity exponent, and K_{Ic} is the fracture toughness of the material. By inserting Eq. (10) in Eq. (11), and integrating, we obtain:

$$\int_{\theta_i}^{\theta_f} \frac{d\theta}{(\mu \sqrt{a/r_0})^n} = v_0 \left(\frac{4E^*}{3R} \right)^{1/3} \left(\frac{3E^*}{\pi R K_{Ic}^2} \right)^{n/2} P^{(3n-2)/6} t \quad (12)$$

where θ is the radial coordinate of the ring crack, θ_i is the initial defect size, that can be taken as 0, and θ_f the final defect size, that in the case that the ring crack is fully developed can be taken as $2\theta_f = 2\pi$. The left size of the equation is adimensional and almost independent of the applied load, for the values of applied load considered here. Therefore, Eq. (12) can be reduced and approximated to:

$$P^{n/2} t = A \quad (13)$$

where A is constant for that given material and indenter.

For the case of a material with residual stress, the value of μ is affected by the relative value of these residual stresses with respect to peak indentation pressure.³⁸ If this relative value is lower than 20%, the modified value of μ by the residual stresses, labelled as μ' , can be related through the value of μ without residual stresses by the approximation:

$$\mu' = \mu b^{-\sigma_r/P^{1/3}} \quad (14)$$

where b is a constant, which depends on the elastic properties of the material and the indenter. Using this relationship for μ' , a similar relationship as Eq. (13) between load and time taking into account the residual stresses can be derived:

$$P^{n/2} b^{-\sigma_r n/2 P^{1/3}} t = A \quad (15)$$

because the value of residual stress in our case is around 6% of the peak pressure value, Eq. (15) can be approximated to:

$$P^{n/2} \left(1 - \frac{\sigma_r n}{2 P^{1/3}} \ln b \right) t = A \quad (16)$$

That is, when residual stresses are small, the experimental data are shifted in comparison with the unstressed material. If the range of loads is not too large, this shift will appear almost constant for all the values of P , and the apparent slopes of the experimental data will appear equal for the stressed and unstressed materials. For larger range of applied loads, the apparent slope will be affected by the residual stresses. It is important to note that the crack velocity exponent n is not affected by the residual stresses, as its value is given by the chemical interaction between the material and the medium.

If the data presented in Fig. 2 is fitted with Eq. (15), a value of $n = 53 \pm 9$ is obtained as a media of the slopes of all three materials. This value is in reasonable agreement with the values of stress corrosion cracking exponent previously reported in literature, between 40¹⁸ and 60.³⁹

We can follow a similar reasoning for the case of cyclic loading of alumina, and arrive to similar relationships as Eq. (13). If we depart from the Paris law:

$$\frac{dc}{dN} = D K_{\max}^m \quad (17)$$

where m is the Paris law exponent, D is a constant and K_{\max} is the maximum applied stress intensity factor, we can arrive at the relationship

$$N_f P_{\max}^{m/2} = B \quad (18)$$

where N_f is the number of cycles to failure, P_{\max} is the maximum applied load and B is a constant. Alternatively, if we start from the modified Paris law:

$$\frac{dc}{dN} = F K_{\max}^p (\Delta K)^q \quad (19)$$

being p and q exponents and F a constant, we arrive to the relationship:

$$\left[P_{\max}^{p/2} (P_{\max}^{1/2} - P_{\min}^{1/2})^q \right] N_f = C \quad (20)$$

with C a constant.

Then the data presented in Fig. 3 can be fitted by Eq. (18), and the mean slope of the three materials can be used to evaluate the value of the exponent of the Paris law, obtaining $m = 22 \pm 4$. The values obtained are in relatively good agreement with literature. For example, Guiu and coworkers^{28,29} report values of m between 13 and 20, Healy et al.³⁰ report a value of m of approximately 30. In a similar way, the data

presented in Fig. 4a and b can be used to obtain the values of p and q , through Eq. (20) without considering residual stresses, giving $p = 19.0 \pm 2.8$ and $q = 2.4 \pm 0.4$, which are again in accordance with literature, where p is always larger than q .

Hence, it is seen that, despite the approximate nature of Eqs. (15), (18) and (20), they yield stress intensity exponents that are relatively similar to values reported in the literature. However, it has to be taken in mind that, first of all, the experimental data do have an inherent high scatter which may affect the value of the exponents and, second, that these equations are approximations for small load ranges and relatively small values of residual stresses at the surface.

It is expected that the analysis of the stress intensity factor of a ring crack growing below critical stress with the existence of biaxial residual stress can be refined in future work. It has not escaped the authors attention that this method, once further developed, can be used to obtain data over stress corrosion cracking and fatigue of any brittle material with a relative low amount of material, a frequent necessity when characterizing advanced materials.¹⁹

4. Conclusions

The Hertzian contact fatigue behaviour (both under static and cyclic loading) of two $\text{Al}_2\text{O}_3\text{-Al}_2\text{O}_3\text{-ZrO}_2$ laminated composites have been characterized and compared to the behaviour of a monolithic alumina with similar microstructure. The contact was performed on the top alumina layer of the laminates, which was in compression, and the appearance of ring crack (not cone crack) was considered as the sign of damage. From the results we can conclude the following:

- (1) Both laminated composites presented much better resistance to contact loading than the monolithic alumina, and the A/2AZ composite, which has a higher residual stress at the surface, presented better resistance than the A/AZ composite. This can be attributed to the existence of biaxial residual compressive stresses at the surface of the laminates, result of the thermal expansion mismatch between the different layers of the composites. This better resistance was present in both cyclic loading and static loading.
- (2) Results from the cyclic loading tests show that the top alumina layer suffered from real fatigue effect, and not only from stress corrosion cracking, because all the materials degraded much faster under cyclic loading than under static loading. This fact was consistent with previous literature reports and attributed to the R-curve behaviour exhibited by alumina due to the presence of crack bridging. This effect is enhanced by a short crack effect, consequence of the dimensions of the crack along the perimeter of the ring crack and, specially along the depth, were it only reached a few micrometers.
- (3) A simple relationship between applied load and time to failure (or, alternatively, number of cycles) was derived, for small variations of load and relatively low residual stress. Despite these approximations, it was found that the stress intensity factors exponents of the Paris law type equations did match within the experimental scatter to values of these exponents previously reported in literature.

Acknowledgments

Work supported in part by the European Community's Human Potential Programme under contract HPRN-CT-2002-00203, [SICMAC] and by the Spanish Ministry of Science and Technology, through grant MAT-2002-00368. L.C. and F.C. acknowledge the financial support provided through the European Community's Human Potential Programme under contract HPRN-CT-2002-00203, [SICMAC]. E.J.P. acknowledges the financial support provided by the Generalitat de Catalunya, grant RED-15/2002. The authors would like to thank Prof. Pavon for fruitful discussions.

References

1. Moya, J. S., Layered ceramics. *Adv. Mater.*, 1995, **7**(2), 185–189.
2. Chan, H. M., Layered ceramics: processing and mechanical behaviour. *Annu. Rev. Mater. Sci.*, 1997, **27**, 249–282.
3. Harner, M. P., Chan, H. M. and Miller, G. A., Unique opportunities for microstructural engineering with duplex and laminar ceramic composites. *J. Am. Ceram. Soc.*, 1992, **75**(7), 1715–1728.
4. Mawdsley, J. R., Kovar, D. and Halloran, J. W., Fracture behaviour of alumina/monazite multilayer laminates. *J. Am. Ceram. Soc.*, 2000, **83**(4), 802–808.
5. Marshall, D. B., Ratto, J. J. and Lange, F. F., Enhanced fracture toughness in layered microcomposites of Ce-ZrO₂ and Al₂O₃. *J. Am. Ceram. Soc.*, 1991, **74**(12), 2979–2987.
6. Sorensen, B. F. and Horsewell, A., Crack growth along interfaces in porous ceramic layers. *J. Am. Ceram. Soc.*, 2001, **84**(9), 2051–2059.
7. Requena, J., Moreno, R. and Moya, J. S., Alumina and alumina/zirconia multilayer composites obtained by slip casting. *J. Am. Ceram. Soc.*, 1989, **72**(8), 1511–1513.
8. Goretta, K. C., Gutierrez-Mora, F., Picciolo, J. J. and Routbort, J. L., Joining alumina/zirconia ceramics. *Mater. Sci. Eng. A*, 2003, **341**, 158–162.
9. Sánchez-Herencia, A. J., James, L. and Lange, F. F., Bifurcation in alumina plates produced by a phase transformation in central alumina/zirconia thin layers. *J. Eur. Ceram. Soc.*, 2000, **20**(9), 1297–1300.
10. Hutchinson, J. W. and Suo, Z., Mixed mode cracking in layered materials. *Adv. Appl. Mech.*, 1992, **29**, 63–191.
11. Moon, R. J., Bowman, K. J., Trumble, K. P. and Rödel, J., Fracture resistance curve behaviour of multilayered alumina-zirconia composites produced by centrifugation. *Acta Mater.*, 2001, **49**, 995–1003.
12. Hatton, B. and Nicholson, P. S., Design and fracture of layered Al₂O₃/TZ3Y composites produced by electrophoretic deposition. *J. Am. Ceram. Soc.*, 2001, **84**(3), 571–576.
13. Rao, M. P., Sánchez-Herencia, A. J., Beltz, G. E., McMeeking, R. M. and Lange, F. F., Laminar ceramics that exhibit a threshold strength. *Science*, 1999, **286**, 102–105.

14. Sánchez-Herencia, A. J., Pascual, C., He, J. and Lange, F. F., ZrO₂/ZrO₂ layered composites for crack bifurcation. *J. Am. Ceram. Soc.*, 1999, **82**(6), 1512–1518.
15. Toschi, F., Melandri, C., Pinasco, P., Roncari, E., Guicciardi, S. and de Portu, G., Influence of residual stresses on the wear behavior of alumina/alumina-zirconia laminated composites. *J. Am. Ceram. Soc.*, 2003, **86**(9), 1547–1553.
16. Lee, S. K. and Lawn, B. R., Contact fatigue in silicon nitride. *J. Am. Ceram. Soc.*, 1999, **82**(5), 1281–1288.
17. Kim, D. K., Jung, Y.-G., Peterson, I. M. and Lawn, B. R., Cyclic fatigue of intrinsically brittle ceramics in contact with spheres. *Acta Mater.*, 1999, **47**(18), 4711–4725.
18. Fett, T., Keller, R., Munz, D., Ernst, E. and Thun, G., Fatigue of alumina under contact loading. *Eng. Fract. Mech.*, 2003, **70**, 1143–1152.
19. Pavón, J. J., Jiménez-Piqué, E., Anglada, M., Saiz, E. and Tomsia, A., Stress corrosion cracking of a glass coating on Ti6Al4V for biomedical applications. *J. Eur. Ceram. Soc.*, submitted for publication.
20. Fiori, C. and de Portu, G., Tape casting: a technique for preparing and studying new materials. In *British Ceramic Proceedings No. 38—Novel Ceramic Fabrication Processes and Applications*, ed. R. W. Davidge, 1986, p. 213.
21. Anstis, G. R., Chantikul, P. and Lawn, B. R., A critical evaluation of indentation techniques for measuring fracture toughness: I, direct crack measurements. *J. Am. Ceram. Soc.*, 1981, **64**, 533–538.
22. Roebben, G., Steen, M., Bressers, J. and van der Biest, O., Mechanical fatigue in monolithic non-transforming ceramics. *Prog. Mater. Sci.*, 1996, **40**, 265–331.
23. Lawn, B. R., Indentation of ceramics with spheres: a century after Hertz. *J. Am. Ceram. Soc.*, 1998, **81**(8), 1977–1994.
24. Warren, P. D., Hills, D. A. and Dal, D. N., Mechanics of Hertzian cracking. *Tribol. Int.*, 1995, **28**(6), 357–362.
25. Rhee, Y.-W., Kim, H.-W., Deng, Y. and Lawn, B. R., Brittle fracture versus quasi plasticity in ceramics: a simple predictive index. *J. Am. Ceram. Soc.*, 2001, **48**(3), 561–565.
26. van der Laag, N. J., Dortmans LJMG and de With, G., Influence of relative humidity on mechanical properties of alumina, PZT and zirconia. *Key Eng. Mater.*, 2002, **206**(2), 751–754.
27. Kim, D. K., Jung, Y.-G., Peterson, I. M. and Lawn, B. R., Cyclic fatigue of intrinsically brittle ceramics in contact with spheres. *Acta Mater.*, 1999, **47**(18), 4711–4725.
28. Li, M. and Guiu, F., Subcritical crack growth in alumina—I. Effects of grain size, specimen size and loading mode. *Acta Metall. Mater.*, 1995, **43**(5), 1859–1869.
29. Guiu, F., Reece, M. J. and Vaughan, D. A. J., Cyclic fatigue of ceramics. *J. Mater. Sci.*, 1991, **26**, 3275–3286.
30. Healy, J., Bushby, A. J., Mai, Y.-W. and Mukhopadhyay, A. K., Cyclic fatigue of long and short cracks in alumina. *J. Mater. Sci.*, 1997, **32**, 741–747.
31. Geraghty, R. D., Hay, J. C. and White, K. W., Fatigue degradation of the crack wake zone in monolithic alumina. *Acta Mater.*, 1999, **47**(4), 1345–1353.
32. Kruzic, J. J., Cannon, R. M. and Ritchie, R. O., Crack-size effects on cyclic and monotonic crack growth in polycrystalline alumina: quantification of the role of grain bridging. *J. Am. Ceram. Soc.*, 2004, **87**(1), 93–103.
33. Jacobs, D. S. and Chen, I.-W., Cyclic fatigue in ceramics: a balance between crack shielding accumulation and degradation. *J. Am. Ceram. Soc.*, 1995, **78**(3), 513–520.
34. Warren, P. D., Hills, D. A. and Dal, D. N., Mechanics of Hertzian cracking. *Tribol. Int.*, 1995, **28**(6), 357–362.
35. Licht, V., Hüselmeier, P. and Fett, T., Probability of cone crack initiation due to spherical indentation due to spherical contact loading. *J. Eur. Ceram. Soc.*, 2004, **24**, 2907–2915.
36. Dai, D. N., Hills, D. A., Warren, P. D. and Nowell, D., The propulsion of surface flaws by elastic indentation testing. *Acta Metall. Mater.*, 1995, **43**(3), 985–991.
37. Warren, P. D., Determining the fracture toughness of brittle materials by Hertzian indentation. *J. Eur. Ceram. Soc.*, 1995, **15**, 201–207.
38. Roberts, S. G., Lawrence, C. W., Birsat, Y., Warren, P. D. and Hills, D. A., Determination of surface residual stresses in brittle materials by Hertzian indentation: theory and experiments. *J. Am. Ceram. Soc.*, 1999, **82**(7), 1809–1816.
39. Barinov, S. M., Ivanov, N. V., Orlov, S. V. and Shevchenko, V. J., Influence of environment on delayed failure of alumina ceramics. *J. Eur. Ceram. Soc.*, 1998, **18**, 2057–2063.